RSC Advances

ROYAL SOCIETY OF CHEMISTRY

www.rsc.org/advances

RSC Advances

RSCPublishing

ARTICLE

Porous NiO nanosheets self-grown on alumina tube using a novel flash synthesis and their gas sensing properties

Cite this: DOI: 10.1039/x0xx00000x

Received 00th January 2012,
Accepted 00th January 2012

DOI: 10.1039/x0xx00000x

www.rsc.org/

Chengjun Dong,[a] Xuechun Xiao,[a] Gang Chen,[a] Hongtao Guan,[a] Yude Wang,*[a] and Igor Djerdj*[b]

Porous NiO nanosheets were self-grown on an alumina tube with a pair of Au electrodes connected by platinum wires via a simple solution combustion synthesis. A cubic NiO phase was obtained by a mixed solution of an oxidizer of nickel nitrate and a fuel of ethylene glycol (EG) at 400 °C. The phases and the morphologies of the materials self-grown on an alumina tube were characterized by X-ray diffraction (XRD), scanning electron microscopy (SEM), and transmission electron microscopy (TEM). The results showed that the alumina tube was entirely covered by NiO nanosheets with several micrometers in thickness. The NiO nanosheets on the surface of the tube were assembled by a large number of nanoparticles of irregular shapes and pores with different sizes. The electronic and gas-sensing characteristics of the self-grown porous NiO nanosheets for volatile organic compound (VOC) vapours (ethanol, acetone, methanol, and formaldehyde) were investigated. The resistance of the sensor directly based on the self-grown NiO dramatically drops from 100-240 °C, and then slightly decreases with further increasing temperature to about 28 kΩ at 400 °C. The sensor based on the self-grown NiO exhibits low detection limit, fast response and recovery and wide dynamic range detection to VOC vapours, especially ethanol, at respectively optimal operating temperature.

1. Introduction

Up to now, intensive studies have been focused on metal oxide gas sensors owing to the demand of sensitive, fast response, and stable sensors for industry, environmental monitoring, biomedicine, and so forth. A variety of oxide semiconductor based gas sensors including SnO_2, ZnO, WO_3, In_2O_3, Fe_2O_3 have been used to detect combustible, flammable, harmful and toxic gases.[1] In contrast to these n-type oxide semiconductors, a relatively little attention has been paid so far to the gas sensors fabricated using p-type oxide semiconductors such as NiO, CuO, Co_3O_4, Cr_2O_3.[2] The remarkably different gas sensing characteristics of n- and p-type oxide semiconductors can be explained in terms of majority charge carriers and gas sensing mechanisms.[2] Hübner *et al.* suggested that the responses of p-type oxide semiconductor sensors to gases was equal to the square root of that of an n-type oxide semiconductors gas sensor to the same gas under the identical morphological configurations.[3] Besides, it is reported that the p-type oxide semiconductors are promising candidates for high performance gas sensors with advantages of low humidity dependence and rapid recovery kinetics due to the distinctive oxygen adsorption.[4] Moreover, combining both p- and n-type oxide semiconductor to form p-n junction can also be an alternative way to improve the gas sensing characteristics.[5] As an important p-type semiconductor, NiO has attracted considerably investigation because of its unique properties such as a wide band-gap (3.6-4.0 eV), a measurable electrical conductivity change accompanied with chemical reactions on the surface of materials, which has a potential application to gas sensors, with many related articles published. Nevertheless, the diverse structures of NiO (nanoparticles, nanosheets, nanotubes, fibers, hollow spheres, nanowires, etc.),[6-10] appropriate doped-NiO (Pt, Au, Fe, and Zn),[12-14] and NiO composites with other oxide semiconductors (ZnO, SnO_2, and PdO)[15-17] have been developed in recent years as a sensitive material for ethanol, acetone, methanol, formaldehyde, CO and NH_3. However, the high sensing performance of NiO based gas sensor is still a challenge, showing a great technological and scientific interest.

Currently, oxide semiconductor sensors can be realized by measuring various signal such as resistance/conductance, ion, mass, or optical change.[18] Particularly, resistance/conductance changes are one of the most common manners, which have been widely employed by using conductive polymers, or metal oxides, or metal as sensing materials. The basic working principle for these sensors are based on the resistance changes (R_a/R_g for n-

type oxide semiconductors, R_g/R_a for p-type oxide semiconductors, R_a: resistance in normal air, R_g: resistance in analyte gas) caused by exposure of the sensor to tested target gaseous species. There are nowadays many distinct methods in fabricating gas sensors. In a typical gas sensor fabrication process, the sensitive materials have been prepared by different chemical synthesis methods firstly. Subsequently, the materials were mixed with suitable amount of water, ethanol or terpineol to form a paste, and then the paste was coated onto a ceramic tubes or SiO_2/Si substrate with a pair of pre-prepared Au or Ti electrodes connected by platinum wires. Also, nanowires were directly grown on SiO_2/Si substrate with patterned metal coatings which acts as both electrodes and catalyst for the growth of the nanowires.[1,18] Meanwhile, another novel approaches of sensor fabrication with advantages of simplicity, mass production, time saving, and cost effective is also a gap needing bridge. Recently, Marks' group developed a new strategy for fabricating optoelectronic devices via a solution-processed using self-energy generating combustion synthesis.[19] The combustion synthesis can yield a localized energy supply to synthesize homogeneous, higher surface area, and high purity products with relatively simple equipment. The essence of combustion synthesis is to utilize the exothermicity of the redox reaction between appropriate oxidizer and fuel to directly crystallize the oxide phase from the mixture of the precursor solution.[20] Upon such a strategy, Jin and co-workers synthesized NiO_x thin films as hole transport interlayer for optoelectronic devices.[21] There are no attempts to use such strategy to fabricate NiO gas sensor.

Herein, the NiO layer was directly self-grown on alumina tube with Au electrodes and platinum wires as gas sensor using solution combustion synthesis. The phase analysis, morphology and microstructures of self-grown NiO were thoroughly characterized at the nanoscale. The gas sensor based on self-grown NiO exhibits fast response and recovery, a low detection limit and wide dynamic range detection for four kinds of VOC vapours including ethanol, acetone, methanol, and formaldehyde. Among them, the sensor is more sensitive to ethanol than to other three gases. Lastly, the mechanism of the sensor is proposed in brief and further plausible improving approaches for gas sensing performance are also suggested.

2. Experimental

2.1. Fabrication of NiO gas sensor

All of the purchased chemical reagents in the experiment were of analytical grade and were used directly as received without any further purification. An alumina tube (4 mm in length and 1.2 mm in diameter) with a pair of Au electrodes and corresponding platinum wires was directly used to grow NiO. Before NiO growth, the alumina tubes were cleaned sequentially with diluted hydrochloric acid, ethanol and deionized water. Depending on the suitable conditions for chemical reaction to take place, nickel nitrate ($Ni(NO_3)_2{\cdot}6H_2O$) was chosen as oxidizer and ethylene glycol (EG) as a fuel. Stoichiometric compositions of the oxidizer and fuel are obtained according to the complete combustion reaction (400 °C) in the following:[22]

$$Ni(NO_3)_2 \cdot 6H_2O + C_2H_6O_2 \xrightarrow{\Delta} NiO + N_2 + 2CO_2 + 9H_2O \quad (1)$$

In a typical synthetic procedure, 10 mmol of $Ni(NO_3)_2{\cdot}6H_2O$ and 10 mmol of EG were dissolved in 15 mL deionized water to make a green solution in a beaker. Next, the solution of combustion precursor was transferred into a crucible, and then the cleaned alumina tubes were placed into the precursor for 10 min. Afterwards, the crucible was put to a preheated furnace at the temperature of 400 °C for 120 min. After the reaction, the crucible with fluffy loose products was taken out and cooled down naturally in atmosphere. Finally, the alumina tubes were picked up from the obtained fluffy loose NiO. A layer of NiO was successfully self-grown on the surface of the alumina tube to form the gas sensor.

2.2. Characterization

The resulting sensor was characterized by X-ray diffraction (XRD, Rigaku TTRIII) with an incident X-ray wavelength of 1.540 Å (CuKα line). Scanning electron microscopy (SEM) analysis was carried out by FEI QUANTA200 with microscope operating at 30 kV. The detailed microstructures of the sample were also determined using transmission electron microscopy (TEM) and high-resolution transmission electron microscopy (HRTEM) (JEOL JEM-2100) with an acceleration voltage of 200 kV. The NiO were carefully peeled off from alumina tube and dispersed in ethanol and dropped on copper grids for measurement.

2.3. Gas sensor testing

The ceramic tube with NiO layer was connected to a Bakelite base by platinum wires and a Ni-Cr alloy was inserted into the tube to ensure a heating temperature control with different heating voltage (V_H). Measurements on the gas sensing properties of the sensor were performed on a WS-30A system (Weisheng Instruments Co. Zhengzhou, China). During the test, a given amounts of target gas was injected into the test chamber with 18 L in volume via a microinjector and mixed with reference gas immediately by a evaporator and two fans in the test chamber. Meanwhile, the clean air was used as a reference gas and diluting gas for the different concentrations of tested gas. As a kind of p-type gas sensor, the sensor response was defined as the ratio of the sensor resistance in target gases (R_g) to that of in normal air (R_a), which was measured at a temperature ranging from 100 to 360 °C. The response and recovery times are defined as the time taken for a 90% change of the final equilibrium value in the adsorption and desorption processes. In order to improve their stability and repeatability, the gas sensors were aged at an operating temperature of 150°C for 150 h in normal air. More details including the schematic structure of the gas sensor as well as the basic testing principle are displayed in Fig. S1 in the Supplementary Material.

3. Results and discussion

After the reaction, the alumina tube has been entirely covered with NiO layer and loose products and the Au electrodes were not visible. Note that the loose products were slightly shaken off. To investigate the structure of the obtained NiO on the surface of alumina tube, XRD measurements were carried out. Fig. 1 illustrates the XRD diffraction pattern of the self-grown NiO. Comparison with the JCPDS card No. 71-1179, the diffraction peaks can be clearly indexed to a cubic NiO phase with the strongest peak being the (200) reflection. As is evident, the obvious five peaks at 37.21°, 43.23°, 62.75°, 75.35°, and 79.36° correspond to (111), (200), (220), (311), and (222) Bragg reflections of NiO. Besides, no other secondary or amorphous phase was found from the XRD patterns, indicating that the NiO was crystallized on the surface of the alumina tube. Therefore, our strategy provides an effective approach to directly grow NiO on the surface of alumina tube to further fabricate the gas sensor.

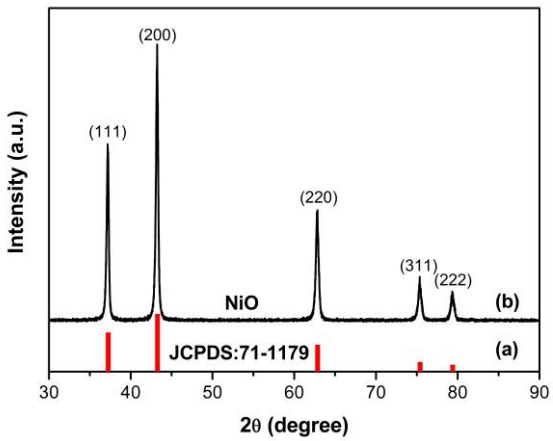

Fig. 1 (a) The vertical line represents the JCPDS:71-1179. (b) X-ray diffraction pattern of NiO self-grown on alumina tube.

The overall and typical surface morphologies as well as cross-section images have been examined by SEM, as shown in Fig. 2. It can be observed that the entire alumina tube has been covered by NiO layer (Fig. 2 (a)). The NiO layer is composed of nanosheets with random distributions of loose products, as shown in SEM (Fig. 2 (b)). By taking a closer look, a large amount of pores are apparently observed on the surface of these NiO nanosheets due to the liberation of gases such as H_2O vapours, CO_2 and N_2 in the combustion process. From the cross-section SEM images in Fig. 2 (c) and (d), the thickness of NiO layer is of about several micrometers. Furthermore, the NiO is compactly adhesive to the alumina tube surface, as displayed in the inset of Fig 2 (d). Thus, the gas sensor is directly prepared through porous NiO nanosheets self-grown on the surface of alumina tube with Au electrodes and platinum wires.

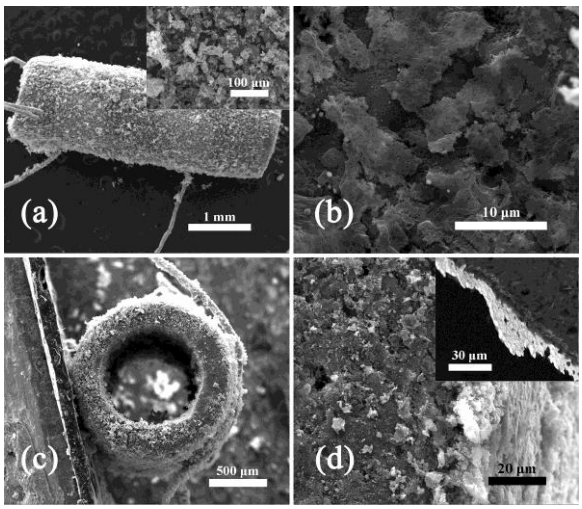

Fig. 2 (a) and (b) are the overall and typical SEM images of self-grown NiO nanosheets on the alumina tube (the inset in (a) shows the low-magnification image of NiO); (c) and (d) are the overall and representative cross-sectional images of NiO gas sensor (the inset in (d) shows the High-magnification cross-section image of NiO sensor).

The TEM and HRTEM images of as-synthesized NiO on the surface of alumina tube provide more information about the structure characteristics. For measurement, the TEM samples were prepared by scratching the NiO layer from alumina tube, followed by dispersing them in ethanol and casting them on the copper grids. As demonstrated in Fig. 3 (a), NiO nanosheet is assembled by a large number of nanoparticles with irregular shape and pores, meanwhile, the nanopores are evidently distributed throughout the nanosheets. From the HRTEM micrograph of NiO nanosheets (Fig. 3 (b)), the size of nanoparticles varies from several nanometers up to tens of nanometers with a smooth surface. From a selected-area electron diffraction (SAED) pattern shown in the Fig. 3 (d), all diffraction rings on this pattern could be exactly attributed to cubic NiO, illustrating a polycrystalline nature, which further supports that the above XRD results. In addition, many porous substructures are obviously detected due to the agglomeration of the irregular nanoparticles. The HRTEM images additionally revealed the locally crystalline nature. A HRTEM image of a nanosheet (Fig. 3 (c)) shows resolved fringes separated by 0.241 nm, which agrees with the d spacing of the (111) crystal planes in cubic NiO. The pores are plausibly believed to form by irregular nanoparticles.

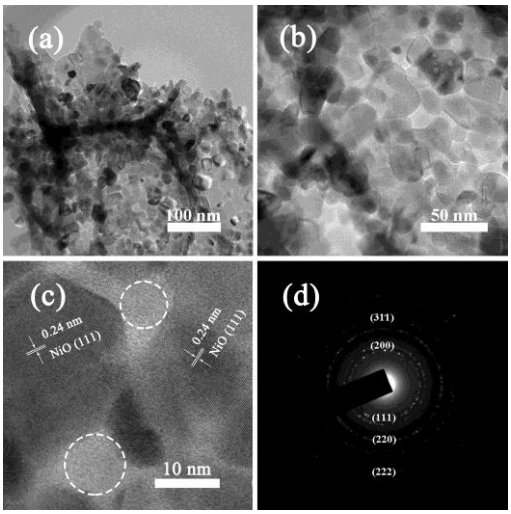

Fig. 3 (a) and (b) are Low-magnification and High-magnification TEM micrograph of a NiO nanosheet, (c) the corresponding HRTEM image (the white dash circles highlight the typical pores), and (d) the selected area electron diffraction pattern (SAED).

Research on conductivity of self-grown NiO gas sensor was performed in normal air at the temperature ranged from 100-400 °C. Variation of resistance (R) with operating temperature for a typical NiO gas sensor is shown in Fig. 4. As observed in this figure, the resistance of the sensor markedly decreases with the increase in temperature, which can be explained by the semiconducting properties of the synthesized NiO. Specifically, a sharp resistance drop from 960-94 kΩ occurs at the operating temperature of 100-240 °C, then it slightly decreases to about 28 kΩ at 400 °C. This resistance variation strongly suggests that the concentration of acceptors increases with the temperature, which is similar with other reports.[23]

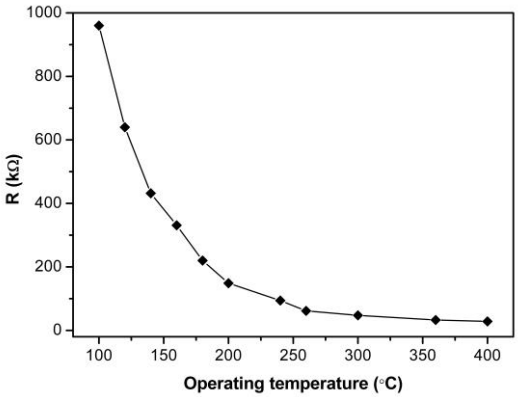

Fig. 4 The resistance variation of self-grown NiO gas sensor at different operating temperature in the range of 100-400 °C in normal air.

In order to test our sensor, four VOC vapours including ethanol, acetone, methanol, and formaldehyde have been attempted. The operating temperature is one of the most important characteristic for the gas sensor, which is determined not only by the nature of the materials itself, but also the gas-sensing process of the gas towards the surface of materials. Therefore, the respectively optimum operating temperature for each gas has been ascertained firstly. Fig. 5 represents the typical relationship between the gas response and the operating temperature of self-grown NiO sensor for different gases with a concentration of 1000 ppm. Obviously, the gas response is both operating temperature and gas dependent. Regardless the gas, the response increases with the rise of the operating temperature at the beginning and then reaches a maximum at an optimal temperature, followed by the decrease of gas response with a further increase of the operating temperature. The best operating temperature for methanol and formaldehyde is the same at 180 °C. However, the optimized operating temperatures are revealed to be 200 °C and 260 °C for ethanol and acetone, respectively. Then, the optimal operating temperature can be applied in all investigations hereinafter. It is worth noting that the sensor is much more sensitive for ethanol than other three tested gases at correspondingly optimal operating temperature. The gas dependent operating temperature can be explained from the kinetics and mechanics of gas absorption and desorption from the surface of NiO. Normally, a certain activation energy provided by increasing the reaction temperature are needed to oxygen absorption on the surface of NiO, thus, a high sensitivity can only be obtained at a suitable temperature.[24] The real-time dynamic responses towards ethanol, acetone, methanol, and formaldehyde with concentrations of 5-1000 ppm at correspondingly optimal operating temperature are displayed in Fig. 6. One can see that the response for all gases increases along with increased gas concentrations. As clearly shown in Fig.6, the response of the sensor increase abruptly and then gradually approaches steady state upon exposure to the target gas. After purging with normal air again, the responses approximately recover to its initial value. This is expected for a p-type semiconductor upon exposure to reducing gas, which is associated with other sensors on the NiO base.[6] The results apparently indicate that even the lowest concentration of ethanol, acetone, methanol, and formaldehyde, i.e. 5 ppm, can be detected. Generally, the response time and recovery time are defined as the time needed to reach 90% of the steady value. It is found that the response and recovery time for self-grown NiO sensor is less than 1 min for all tested gases on each concentration, which demonstrates that the sensor possess fast response and recovery properties.

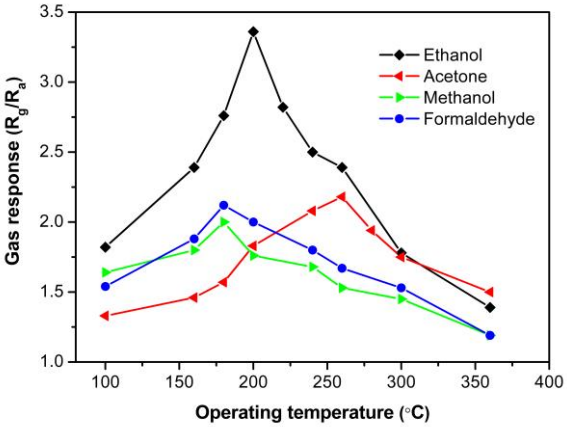

Fig. 5 Dependence of gases (ethanol, acetone, methanol, and formaldehyde) response on operating temperature at a gas concentration of 1000 ppm.

The sensing responses as a function of gas concentrations from 5 ppm to 1000 ppm for four tested gases are summarily plotted in Fig. 7. It can be seen that the responses (R_g/R_a) of the as self-grown NiO sensor are dramatically enhanced with the increasing concentration of the tested gas below 300 ppm at respectively optimal operating temperature.

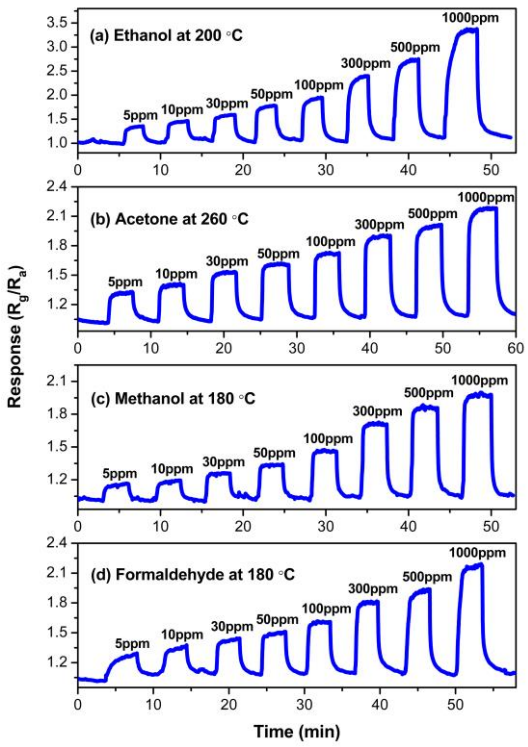

Fig. 6 Featured response and recovery characteristic curve versus time based on the self-grown NiO sensor towards different concentrations of gas in the range 5-1000 ppm at optimal operating temperature.

In contrast, the responses increase slowly above 300 ppm of gases, which may be attributed to the insufficiency of negatively charged oxygen ions on the sensor to oxidize all analysed gases

near the sensor surface and the full adsorption of gas molecules on the sensor.[25] For the self-grown NiO sensor, the response is highest for ethanol, followed by acetone, formaldehyde, and methanol on each concentration. Taking gas concentration of 1000 ppm for example, the responses are 3.4, 2.2, 2.1, and 2.0 for ethanol, acetone, formaldehyde, and methanol, respectively.

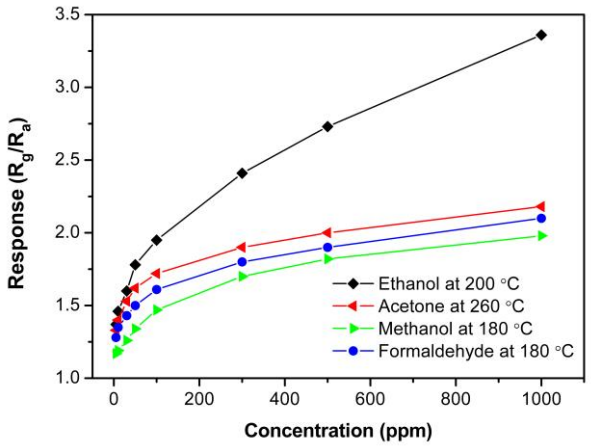

Fig. 7 The response versus gas (ethanol, acetone, methanol, and formaldehyde) concentrations at respective optimum operating temperature for the NiO gas sensor.

It is well known that gas sensing properties of metal oxides depend on several processes in terms of surface adsorption and desorption and diffusion of gases.[26] Thus, the sensitivity and selectivity of gas sensors is greatly affected by morphology and the nature of the sensor materials. In normal air, the oxygen adsorbed on the NiO trapped conduction electrons of the oxide and thus induced a charge-accumulation space charge layer at the surfaces of NiO nanograins. Previous studies related to the oxygen adsorption over NiO surface suggested that O^- is dominating up to 150-200 °C. Above 200 °C, O^{2-} is the main species.[27] Therefore, the adsorbed oxygen could be a great number of O^-, and O^{2-} determined by the activation energies on the surface of NiO.[6,11] During the sensing process, the target gases decomposition reaction on the surface of the NiO can be possibly expressed as following:

$$gas + O^-/O_2^-/O^{2-} \rightarrow CO_2 + H_2O + e^- \quad (2)$$

After exposure to the reducing gases, the adsorbed oxygen was consumed, leading to a decrease in the thickness of the space charge layer. The adsorbed oxygen acts as a sort of acceptor to target gas brought about a resistance change, thereby reflection the species and concentrations of tested gas.

Summing up the above results, the self-grown NiO sensor can be used for the gas detection, such as ethanol, acetone, methanol, and formaldehyde. Among them, the response is highest for ethanol against acetone, formaldehyde, and methanol. This direct approach for gas sensor fabrication takes the advantages of simplicity, low cost, and time saving of solution combustion synthesis. So far, many functional materials have been successfully synthesized via combustion synthesis.[19,28,29] Therefore, sensors based on other highly sensitive materials such as SnO_2, ZnO, In_2O_3, and Fe_2O_3, can be attempted to directly self-grow on the alumina tube with electrodes and connection wires using this novel flash synthesis. Besides, the response of self-grown NiO sensor is still far away from application, hence appropriate dopants such as Fe,[13] and Zn,[14] functionalized with noble metal, i.e. Pt,[11] and Au,[12] and composited with n-type semiconductor like SnO_2,[15] ZnO,[16] PdO,[17] are plausible routes to further improve the gas sensing performance.

4. Conclusions

In summary, porous NiO nanosheets were directly self-grown on an alumina tube with two Au electrodes and platinum wires by a facile solution combustion synthesis. It was found that the oxidizer of $Ni(NO_3)_2 \cdot 6H_2O$ and a fuel of EG favours the formation of cubic NiO at 400 °C. After reaction, the alumina tube was overall covered by a layer of NiO nanosheets comprised of nanoparticles and pores in irregular shape and size. The thickness of the NiO layer was estimated to be about several micrometers. The sensor based on the porous NiO nanosheets was investigated. With the increase of the operating temperature from 100-400 °C, the resistance of the sensor abruptly drops and then tends to be stable. The gas sensor showed a low detection limit for four tested gases including ethanol, acetone, methanol, and formaldehyde. At the correspondingly optimal operating temperature, the sensor exhibited better gas sensing performance towards the ethanol than other three analyte gases in a wide range from 5 ppm to 1000 ppm.

Acknowledgements

This work was supported by the Department of Science and Technology of Yunnan Province via the Key Project for the Science and Technology (Grant No. 2011FA001), National Natural Science Foundation of China (Grant No. 51262029), the Key Project of the Department of Education of Yunnan Province (ZD2013006), and Program for Excellent Young Talents, Yunnan University (XT412003). Igor Djerdj acknowledges financial support from the Unity through Knowledge Fund (www.ukf.hr) of the Croatian Ministry of Science, Education and Sports (Grant Agreement No. 7/13).

Notes and references

[a]Department of Materials Science and Engineering, Yunnan University, 650091 Kunming, Peoples' Republic of China. Fax: +86-871-65153832; Tel: +86-871-65031124; E-mail: ydwang@ynu.edu.cn.

[b]Ruđer Bošković Institute, Bijenička 54, 10000 Zagreb, Croatia. Fax: +38514680114; Tel: +38514680113; E-mail: igor.djerdj@irb.hr.

1. Y. F. Sun, S. B. Liu, F. L, Meng, J. Y. Liu, Z. Jin, L. T. Kong, and J. H. Liu, *Sensors*, 2012, **12**, 2610.
2. H. J. Kim, J. H. Lee, *Sens. Actuators*, B, 2014, **192**, 607.
3. M. Hübner, C. E. Simion, A. Tomescu-Stănoiu, S. Pokhrel, N. Barsan, U. Weimar, *Sens. Actuators*, B, 2011, **153**, 347.
4. H. R. Kim, A. Haensch, I. D. Kim, N. Barsan, U Weimar, J. H. Lee, *Adv. Funct. Mater*., 2011, **21**, 4456.
5. Z. Zhang, C. Shao, X. Li, C. Wang, M. Zhang, Y. Liu, *ACS Appl. Mater. Interfaces*, 2010, **2**, 2915.
6. G. X. Zhu, C. Y. Xi, H. Xu, D. Zheng, Y. J. Liu, X. Xu, and X. P. Shen, *RSC Adv*., 2012, **2**, 4236.
7. N. D. Hoa and S. A. El-Safty, *Chem. Eur. J.*, 2011, **17**, 12896.
8. B. Liu, H. Yang, H. Zhao, L. An, L. Zhang, R. Shi, L. Wang, L. Bao and Y. Chen, *Sens. Actuators*, B, 2011, **156**, 251.

9. N. G. Cho, H. S. Woo, J. H. Lee and I. D. Kim, *Chem. Commun*., 2011, **47**, 11300.
10. N. G. Cho, I. S. Hwang, H. G. Kim, J. H. Lee, and I. D. Kim, *Sens. Actuators B*, 2011, **155**, 366.
11. J. C. Fu, C. H. Zhao, J. L. Zhang, Y. Peng, and E. Q. Xie, *ACS Appl. Mater. Interfaces*, 2013, **5**, 7410.
12. G. Mattei, P. Mazzoldi M. L. Post, D. Buso, M. Guglielmi and A. Martucci, *Adv. Mater*., 2007, **19**, 561.
13. H. J. Kim, K. Choi, K. M. Kim, C. W. Na, J. H. Lee, *Sens. Actuators B*, 2012, **171**, 1029.
14. J. Wang, L. M. Wei, L. Y. Zhang, J. Zhang, H. Wei, C. H. Jiang, and Y. F. Zhang, *J. Mater. Chem*., 2012, **22**, 20038.
15. L. L. Wang, J. N. Deng, T. Fei, T. Zhang, *Sens. Actuators B*, 2012, **164**, 90.
16. L. Xu, R. F. Zheng, S. H. Liu, J. Song, J. S. Chen, B. Dong, and H. W. Song, *Inorg. Chem*., 2012, **51**, 7733.
17. L. L. Wang, Z. Lou, R. Wang, T. Fei, and T. Zhang, *J. Mater. Chem*., 2012, **22**, 12453.
18. X. P. Chen, C. K. Y. Wong, C. A. Yuan, G. Q. Zhang, *Sens. Actuators B*, 2013, **177**, 178.
19. M. G. Kim, M. G. Kanatzidis, A. Facchetti, and T. J. Marks, *Nat. Mater*., 2011, **10**, 382.
20. K.C. Patil, S.T. Aruna, T. Mimani, *Curr. Opin. Solid State Mater. Sci*., 2002, **6**, 507.
21. S. Bai, M. T. Cao, Y. Z. Jin, et al., *Adv. Eng. Mater*., 2014, **4**, 1301460.
22. S. R. Jain, and K. C. Adiga, *Combust. Flame*, 1981, **40**, 71.
23. A. Hakim, J. Hossain, K.A. Khan, *Renew. Energy*, 2009, **34**, 2625.
24. C. X. Wang, L. W. Yin, L. Y. Zhang, D. Xiang, and R. Gao, *Sensors*, 2010, **10**, 2088.
25. Z. J. Wang, Z. Y. Li, J. H. Sun, H. N. Zhang, W. Wang, W. Zheng and C. Wang, *J. Phys. Chem. C*, 2010, **114**, 6100.
26. G. F. Fine, L. M. Cavanagh, A. Afonja, and R. Binions, *Sensors*, 2010, **10**, 5469.
27. A Bielański, M. Najbar, *J. Catal*., 1972, **25**, 398.
28. W Wen, J. M. Wu, Y. D. Wang, *Appl. Phys. Lett*., 2012, **100**, 262111.
29. X. Y. Tao, X. N. Wang, X. D. Li, *Nano Lett*., 2007, **10**, 3172.

